Materials Science

AIMS Materials Science, 7(6): 902–910.
DOI: 10.3934/matersci.2020.6.902
Received: 25 November 2020
Accepted: 25 November 2020
Published: 22 December 2020

http://www.aimspress.com/journal/Materials

Research article

Theoretical study of Ni doping $SrTiO_3$ using a density functional theory

Z. Aboub[1,*], B. Daoudi[1,2], and A. Boukraa[1]

[1] Laboratoire LENREZA, Université Kasdi Merbah-Ouargla, 30000 Ouargla, Algérie
[2] Département Automatique et électromécanique, Faculté des sciences et technologie, Université de Ghardaia

* **Correspondence:** Email: aboubz@yahoo.com.

Abstract: The structural and electronic properties of the Ni-doped $SrTiO_3$ have been study by using the full-potential (Linearized augmented plane-wave method (FP-LAPW) within density functional theory (DFT). We employed the generalized gradient approximation (GGA) and modified Beck-Johnson (mBJ) GGA. The calculated band gaps are found to be decreased with the increase in In concentration. The mBJ-GGA band gaps are very close to experimental values as implemented in the WIEN2k simulation code. We studied the electronic properties of $SrTiO_3$ and effect doping Ni on its. This study revealed that Ni doping of $SrTiO_3$ had a significant impact on the structural and electronic properties of $SrTiO_3$, and its structural stability can be improved by Ni doping $SrTiO_3$. The band gap of $SrTiO_3$ is 2.857 eV and 1.078 eV for $SrNi_{0.125}Ti_{0.875}O_3$.

Keywords: density functional theory; $SrTiO_3$; doping; electronic structure; WIEN2k code

1. Introduction

Photocatalytic water splitting using semiconductor materials provides a way to produce clean hydrogen fuel [1–4]. A photocatalytic water splitting has to be proper band positions, i.e., the valence band maximum V_{BM} should be more positive than the water oxidation potential and the conduction band minimum C_{BM} must be more negative than the hydrogen reduction potential, the $SrTiO_3$ has benne a most stability and an abundance of raw materials, and thus it is a promising photocatalyst for producing hydrogen from water using solar energy [5,6]. $SrTiO_3$ is a cubic perovskite structure material [7]. However, $SrTiO_3$ use at range of applications in many fields such

as, photocatalysis [8–10], energy storage [11,12], sensing [13], micro wave devices[14], anode material for lithium-ion batteries [15], H_2S solar cells [16], and random access memories[17]. Can be synthesize $SrTiO_3$ by several methods such as sol-gel [18], treatment hydrothermal [8,10,13,19,20], solid state reaction [15], polymeric precursor method [9], pulsed laser decomposition [21,22], co-precipitation/solvo-thermal [15], and electro-spinning [23]. And many studies have been done about metal-doped $SrTiO_3$, such as Fe, La and Mn [24–26].

In this work, the structural and electronic properties of both $SrTiO_3$ and $SrNi_{0.125}Ti_{0.875}O_3$ were calculated by using the full potential augmented plane wave plus local orbital (FP-(APW + lo)) method based on density functional theory (DFT) [27]. This is implemented in wien2k code to solve Kohn Sham equation within Full Potential Linearized Augmented Plane Wave (FP-LAPW) method. This method is one of the best methods for appropriate computation of electronic states of various crystalline solids. For structural optimization and the electronic properties the exchange correlation approximation is treated with Perdew-Burke-Ernzerhof Generalized Gradient Approximation (PBE-GGA) Trans-Blaha modified Becke–Johnson (TB-mBJ) potential is employed [28–31].

The outline of this paper is as follows: in section computational details, we give the computation details. The results and discussion are presented in section results and discussion. Finally section conclusions concludes the paper.

2. Computational details

All calculations were performed in the framework of the density function theory (DFT) [27] using the WIEN2k package [32], the full-potential Linearized augmented plane-wave method (FP-LAPW) [27] and the generalized-gradient approximation PBE-GGA with the exchange-correlation functional suggested by Perdew, Burke, and Ernzerhof (PBE) [27].

In these computations, and in order to investigate the structural and electronic properties of $SrTiO_3$ and $SrNi_{0.125}Ti_{0.875}O_3$, the unit cell is separated in two regions, an interstitial region and non-overlapping atomic spheres. In each of these regions, Kohn-Sham wave functions and charge densities as well as electronic potentials are calculated in a different way inside the unit cell. Inside the atomic sphere, they are defined usually by the RMT (radius of muffin tin) around the position of each atom, a spherical harmonic expansion is used, whereas in the interstitial space of the unit cell a plane wave basis set is taken into account. RMT values were chosen as 1.65 a.u. for O, 1.75 a.u. for Ti, 1.8 a.u. for Ni and 2.2 a.u. for Sr. Charge density was Fourier expanded up to $G_{max} = 12$ au^{-1}. The plane wave cut-off $K_{max} \times R_{MT}$ radius was taken such that $R_{MT} \times K_{max} = 9$. For convergence of energy we used a $7 \times 7 \times 7$ k-points grid in the special irreducible Brillouin zone. The self-consistent convergence criteria of total energy calculations of the system were achieved when the total energy stabilized within 10^{-4} Ry.

3. Results and discussion

3.1. Structural analysis

For the calculion of structural and electronic properties of Ni doped $SrTiO_3$, we adopt for the $SrTiO_3$ compound—a cubic structure (space group). Pm3m where atomic positions in the elementary cell as presented in Figure 1a are Sr: (0, 0, 0); O: (0, 1/2, 1/2),(1/2, 1/2, 0), (1/2, 0, 1/2); and Ti:

(1/2, 1/2, 1/2) When, for the Ni-doped compound $SrNi_{0.125}Ti_{0.875}O_3$, we build a cubic super-cell having twice the cell parameter of the parent $SrTiO_3$ compound Figure 1b whose atomic positions are listed in Table 1.

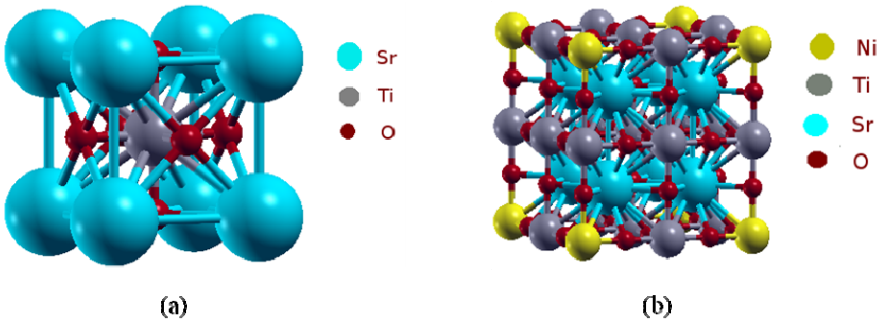

Figure 1. (a) $SrTiO_3$ perovskite structure, and (b) supercell of $SrNi_{0.125}Ti_{0.875}O_3$ structure.

Table 1. Atomic positions for cubic supercell $SrNi_{0.125}Ti_{0.875}O_3$.

Atom	Positions
Sr	(0.75, 0.75, 0.75)(0.25, 0.25, 0.25)(0.25, 0.75, 0.75)(0.75, 0.25, 0.25)(0.25, 0.25, 0.75)(0.75, 0.75, 0.25)(0.75, 0.25, 0.75)(0.25, 0.75, 0.25)
Ni	(0, 0, 0)
Ti	(0.5,0.0, 0.0)(0.0, 0.5, 0.0)(0.0, 0.0, 0.5)(0.0, 0.5, 0.5)(0.5, 0.0, 0.5)(0.5, 0.5, 0.0)(0.5, 0.5, 0.5)
O	(0.0, 0.0, 0.75)(0.0, 0.0, 0.25)(0.75, 0.0, 0.0)(0.25, 0.0, 0.0)(0.0, 0.75, 0.0)(0.0, 0.25, 0.0)(0.5, 0.0, 0.75)

All calculations were performed for a 40 atom (5 × 8) super-cell (with a_0 = 7.81 Å) (Figure 1b). The optimization of the lattice constants for $SrTiO_3$ and $SrNi_{0.125}Ti_{0.875}O_3$ is made by minimization of the total energy. The calculate lattice parameters, bulk moduli, pressure derivatives B' for $SrTiO_3$ and $SrNi_{0.125}Ti_{0.875}O_3$ were calculated by fitting the total energy E versus volume V data to the non-linear Murnagham equation of state [27]. We present the E (V) relationship of both $SrTiO_3$ and $SrNi_{0.125}Ti_{0.875}O_3$ in Figure 2a,b respectively.

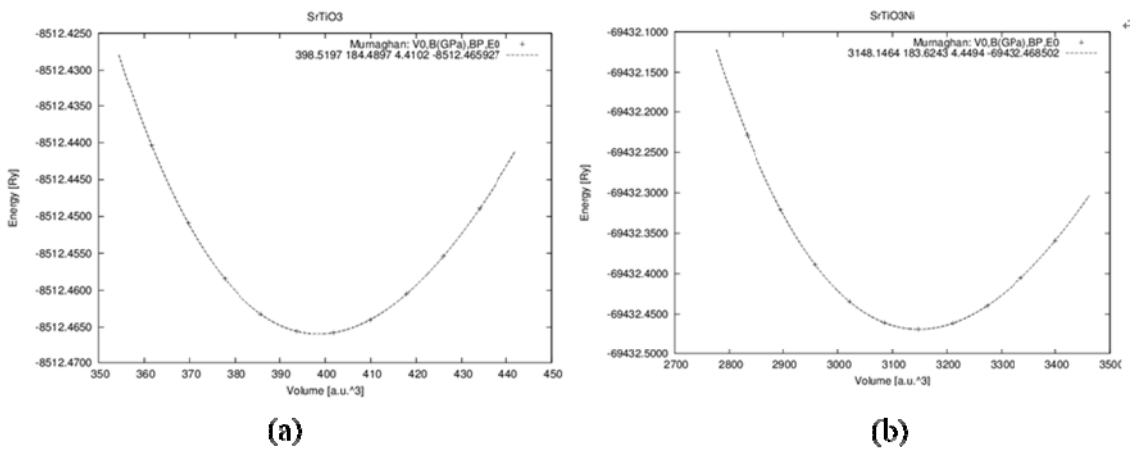

Figure 2. Calculated total energy curves as a function of cell volume for (a) $SrTiO_3$ and (b) $SrNi_{0.125}Ti_{0.875}O_3$.

Table 2 presents the calculate lattice parameters, bulk moduli, their pressure derivatives B' together with available experimental data and other theoretical data for both $SrTiO_3$ and $SrNi_{0.125}Ti_{0.875}O_3$. The value of our calculated lattice constants for both $SrTiO_3$ (3.894 Å) and $SrNi_{0.125}Ti_{0.875}O_3$ (3.877 Å). This is in good agreement with the experiment results [7] that the lattice constant of $SrNi_{0.125}Ti_{0.875}O_3$ films increase after doping. From the values of bulk moduli, we can conclude that the $SrNi_{0.125}Ti_{0.875}O_3$ is slightly less stable than $SrTiO_3$.

Table 2. Calculated lattice constants, bulk moduli B, pressure derivatives B' and compared to experimental data and other available works for $SrTiO_3$ and $SrNi_{0.125}Ti_{0.875}O_3$.

Compounds	Method	Approximation	Lattice constant (Å)	B (GPa)	B'	Refs.
$SrTiO_3$	FP-LAPW	PBE-GGA	3.894	184.489	4.41	Present
	Experimental	Experimental	3.905	/	/	[7]
	FP-LAPW	GGA-96	3.905	184	/	[33]
			3.87	194	/	[34]
$SrNi_{0.125}Ti_{0.875}O_3$	FP-LAPW	PBE-GGA	3.877	183.62	4.44	Present

3.2. Electronic properties

3.2.1. Density of states

In this section, the electronic structures for both $SrTiO_3$ and $SrNi_{0.125}Ti_{0.875}O_3$ will be studied and compared to each other. Several indicators will be used to detect the effects of Ni doping on the $SrTiO_3$ electronic composition, which is total DOS and states partial density (PDOS). From these tools, some aspects of structural features can be demonstrated. The total DOS and PDOS for $SrTiO_3$ are first calculated for comparison and the results are shown in Figure 3a. For clarity, only the Ti 3d, O 2p and Sr 5p PDOS are shown and this will be evident in the following figures. The top of the valence bands (VBs) mainly consists of O 2p states and the most important vacancy power bands in the lower conduction bands (CBs) mainly consist of Ti 3d states. There is no interference between PDOS between Sr atoms and O atoms, meaning that the Sr–O bonds have a high ion city. Furthermore, the band gap in $SrTiO_3$ is about 2.857 eV, which is less than the experimental value (of about 3.2 eV) [32]. This is naturally underestimated by the DFT [35–36] and by cause the strong self-interaction of the Ti 3d states [37] (Figure 3).The total DOS and PDOS for $SrNi_{0.125}Ti_{0.875}O_3$ are shown in (Figure 3) .Where we see the control of both the Ti 3d, Ni 3d, O 2p and Sr 5p PDOS are shown and this will be evident in the following figures. The top of the valence bands (VBs) mainly consists of Ni 3d and O 2p states and the most important vacancy power bands in the lower conduction bands (CBs) mainly consist of Ti 3d states. We also notice no overlap between PDOS Sr atoms and O atoms, meaning that the Sr–O bonds have a high ion. Furthermore, the band gap in $SrNi_{0.125}Ti_{0.875}O_3$ is about 1.078 eV. From all this we conclude that Ni atoms reduce the band gap and improve the effectiveness of $SrTiO_3$.

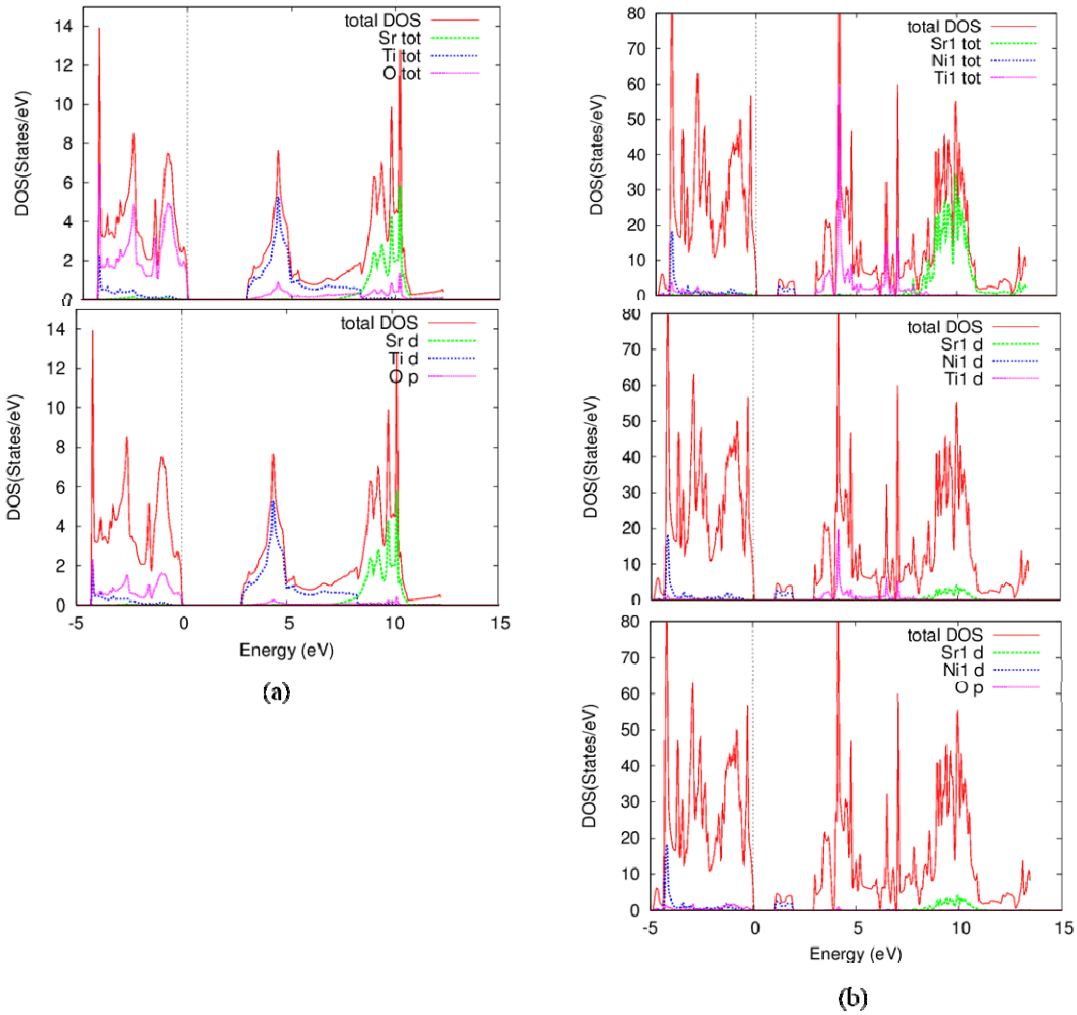

Figure 3. The calculated total and partial density of states for (a) $SrTiO_3$ and (b) $SrNi_{0.125}Ti_{0.875}O_3$.

3.2.2. Band structure

We calculated the band structures of $SrTiO_3$ (Figure 4), and the effect for all doping by nickel metal atoms on the electronic properties of $SrTiO_3$. We found that the $SrTiO_3$ has an indirect gap Γ–M point of Brillouin zone, and our calculated value of this gap (about 2.857 eV) is lower than the experimental value (around 3.2 eV). The largely, due to the well-known shortcoming of exchange-correction functionals in describing, excited states using the PBE-GGA approximation [38,39]. However, the characters of band structures and the relative variation of band gap are reasonable and reliable, so a scissors worker (1.3 eV) was performed to correct the underestimation of the band gaps of doped $SrTiO_3$ [35–40]. Figure 4 shows the calculated band structures $SrNi_{0.125}Ti_{0.875}O_3$ and $SrTiO_3$ around band gap states. Because 1.078 eV, which is an indirect gap (Γ–M point of Brillouin zone). Two isolated defect bands crossing the Brillouin zone make a great decrease to the band gap, thus the optical absorption edge towards the visible light region is largely expanded. The defect bands are close to the valence band, which indicates that Ni dopant atoms are the acceptor impurities, leading to the increase of whole concentration [39].

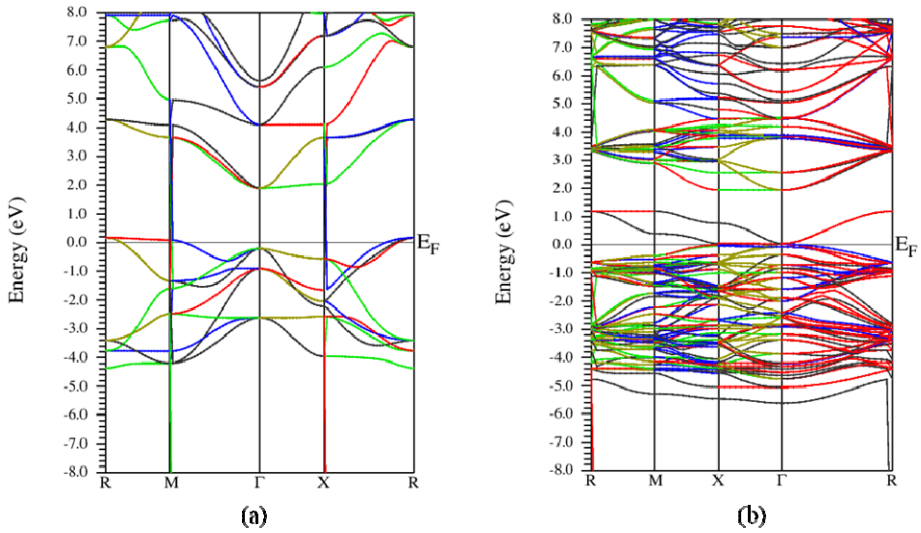

Figure 4. Electronic band structure of (a) $SrTiO_3$ and (b) $SrNi_{0.125}Ti_{0.875}O_3$.

3.2.3. Charge density

Figure 5 represents the charge density of $SrNi_{0.125}Ti_{0.875}O_3$ and $SrTiO_3$. The Sr, Ti, and Ni atoms contain more basic electrons, resulting in a higher overall density of charge near the nucleus position, while oxygen atoms are larger with a large number of valence electrons. In the compounds $SrTiO_3$ and $SrNi_{0.125}Ti_{0.875}O_3$, we note a difference in ionic bonds between Ni–O and Ti–O. This is due to the electronic distribution of Ni and Ti atoms.

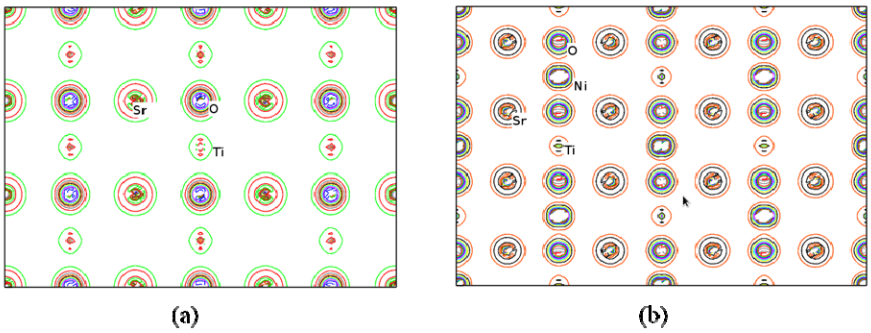

Figure 5. Charge density on the (111) plane for (a) $SrTiO_3$ and (b) $SrNi_{0.125}Ti_{0.875}O_3$.

4. Conclusion

We investigated the structural and electronic properties of Ni-doped $SrTiO_3$ by a first-principles calculation of FP-LAPW method based on DFT. The calculated results the structure of $SrNi_{0.125}Ti_{0.875}O_3$ is less stable than that of pure $SrTiO_3$. The Ni fully acts as an electron donor in $SrNi_{0.125}Ti_{0.875}O_3$ and the Fermi level shifts into the CBs after Ni doping. The DOS of the $SrNi_{0.125}Ti_{0.875}O_3$ system shift toward low energies and the band gap of $SrTiO_3$ is 2.857 eV and reduced by about 1.779 eV for $SrNi_{0.125}Ti_{0.875}O_3$.

Conflict of interests

The authors declare that they have no known competing financial interests or personal relationships that could have appeared to influence the work reported in this paper.

References

1. Tong H, Ouyang S, Bi Y, et al. (2012) Nano-photocatalytic materials: possibilities and challenges. *Adv Mater* 24: 229–251.
2. Osterloh FE (2008) Inorganic materials as catalysts for photochemical splitting of water. *Chem Mater* 20: 35–54.
3. Chen X, Shen S, Guo L, et al. (2010) Semiconductor-based photocatalytic hydrogen generation. *Chem Rev* 110: 6503–6570.
4. Kudo A, Miseki Y (2009) Heterogeneous photocatalyst materials for water splitting. *Chem Soc Rev* 38: 253–278.
5. Hara S, Yoshimizu M, Tanigawa S, et al. (2012) Hydrogen and oxygen evolution photocatalysts synthesized from strontium titanate by controlled doping and their performance in two-step overall water splitting under visible light. *J Phys Chem C* 116: 17458–17463.
6. Reunchan P, Ouyang S, Umezawa N, et al. (2013) Theoretical design of highly active $SrTiO_3$-based photocatalysts by a codoping scheme towards solar energy utilization for hydrogen production. *J Mater Chem A* 1: 4221–4227.
7. Van Benthem K, Elsässer C, French R (2001) Bulk electronic structure of $SrTiO_3$: Experiment and theory. *J Appl Phys* 90: 6156–6164.
8. Niishiro R, Tanaka S, Kudo A (2014) Hydrothermal-synthesized $SrTiO_3$ photocatalyst codoped with rhodium and antimony with visible-light response for sacrificial H_2 and O_2 evolution and application to overall water splitting. *Appl Catal B-Environ* 150: 187–196.
9. Chang CH, Shen YH (2006) Synthesis and characterization of chromium doped $SrTiO_3$ photocatalyst. *Mater Lett* 60: 129–132.
10. Zheng Z, Huang B, Qin X, et al. (2011) Facile synthesis of $SrTiO_3$ hollow microspheres built as assembly of nanocubes and their associated photocatalytic activity. *J Colloid Interf Sci* 358: 68–72.
11. Wang Z, Cao M, Yao Z, et al. (2014) Effects of Sr/Ti ratio on the microstructure and energy storage properties of nonstoichiometric $SrTiO_3$ ceramics. *Ceram Int* 40: 929–933.
12. Shen ZY, Li YM, Luo WQ, et al. (2013) Structure and dielectric properties of $Nd_xSr_{1-x}TiO_3$ ceramics for energy storage application. *J Mater Sci-Mater El* 24: 704710.
13. Kajale DD, Patil GE, Gaikwad V, et al. (2012) Synthesis of $SrTiO_3$ nanopowder by sol-gel-hydrothemal method for gas sensing application. *S2IS* 5: 382–400.
14. Kumar AS, Suresh P, Kumar MM, et al. (2010) Magnetic and ferroelectric properties of Fe doped $SrTiO_{3-\delta}$ films. *J Phys Conf Ser* 200: 092010.
15. Johnson DC, Prieto AL (2011) Use of strontium titanate ($SrTiO_3$) as an anode material for lithium-ion batteries. *J Power Sources* 196: 7736–7741.
16. Burnside S, Moser JE, Brooks K, et al. (1999) Nanocrystalline mesoporous strontium titanate as photoelectrode material for photosensitized solar devices: increasing photovoltage through flatband potential engineering. *J Phys Chem B* 103: 9328–9332.

17. Waser R, Aono M (2007) Nanoionics-based resistive switching memories. *Nat Mater* 6: 833–840.
18. Zhang Y, Hu J, Cao E, et al. (2012) Vacancy induced magnetism in $SrTiO_3$. *J Magn Magn Mater* 324: 1770–1775.
19. Tsumura T, Matsuoka K, Toyoda M (2010) Formation and annealing of $BaTiO_3$ and $SrTiO_3$ nanoparticles in KOH solution. *J Mater Sci Technol* 26: 33–38.
20. Rangel-Hernandez Y, Rendón-Angeles J, Matamoros-Veloza Z, et al. (2009) One-step synthesis of fine $SrTiO_3$ particles using $SrSO_4$ ore under alkaline hydrothermal conditions. *Chem Eng J* 155: 483–492.
21. Kim HS, Bi L, Dionne G, et al. (2008) Magnetic and magneto-optical properties of Fe-doped $SrTiO_3$ films. *Appl Phys Lett* 93: 092506.
22. Egilmez M, Leung G, Hakimi A, et al. (2010) Origin of magnetism in La and Fe doped $SrTiO_{3-\delta}$ films. *J Appl Phys* 108: 123912.
23. Zhang W, Li HP, Pan W (2012) Ferromagnetism in electrospun Co-doped $SrTiO_3$ nanofibers. *J Mater Sci* 47: 8216–8222.
24. Dong XL, Zhang KH, Xu MX (2018) First-principles study of electronic structure and magnetic properties of $SrTi_{1-x}M_xO_3$ (M = Cr, Mn, Fe, Co, or Ni). *Frontiers Phys* 13: 137106.
25. Gillani S, Ahmad R, Rizwan M, et al. (2020) First-principles investigation of structural, electronic, optical and thermal properties of Zinc doped $SrTiO_3$. *Optik* 201: 163481.
26. Zhou X, Shi J, Li C (2011) Effect of metal doping on electronic structure and visible light absorption of $SrTiO_3$ and $NaTaO_3$ (Metal = Mn, Fe, and Co). *J Phys Chem C* 115: 8305–8311.
27. Perdew JP, Burke K, Ernzerhof M (1996) Generalized gradient approximation made simple. *Phys Rev Lett* 77: 3865–3868.
28. Schwarz K, Blaha P (2003) Solid state calculations using WIEN2k. *Comp Mater Sci* 28: 259–273.
29. Blaha P, Schwarz K, Madsen GK (2002) Electronic structure calculations of solids using the WIEN2k package for material sciences. *Comput Phys Commun* 147: 71–76.
30. Kohn W, Sham LJ (1965) Self-consistent equations including exchange and correlation effects. *Phys Rev* 140: 1133.
31. Tran F, Blaha P (2009) Accurate band gaps of semiconductors and insulators with a semilocal exchange-correlation potential. *Phys Rev Lett* 102: 226401.
32. Blaha P, Schwarz K, Madsen G, et al. (2001) *WIEN2k*, *An Augmented Plane Wave + Local Orbitals Program for Calculating Crystal Properties*, Austria: Vienna University of Technology.
33. Benrekia A, Benkhettou N, Nassour A, et al. (2012) Structural, electronic and optical properties of cubic $SrTiO_3$ and $KTaO_3$: Ab initio and GW calculations. *Physica B* 407: 2632–2636.
34. Johnston K, Castell MR, Paxton AT, et al. (2004) $SrTiO_3$ (001) (2 × 1) reconstructions: First-principles calculations of surface energy and atomic structure compared with scanning tunneling microscopy images. *Phys Rev B* 70: 085415.
35. Yang YT, Wu J, Cai YR, et al. (2008) First principles investigation on conductivity mechanism of p-type K: ZnO. *Acta Phys Sin* 51: 7151–7156.
36. Jones RO, Gunnarsson O (1989) The density functional formalism, its applications and prospects. *Rev Mod Phys* 61: 689–746.
37. Burstein E (1954) Anomalous optical absorption limit in InSb. *Phys Rev* 93: 632.

38. Wei W, Dai Y, Jin H, et al. (2009) Density functional characterization of the electronic structure and optical properties of Cr-doped $SrTiO_3$. *J Phys D Appl Phys* 42: 055401.
39. Asahi R, Morikawa T, Ohwaki T, et al. (2001) Visible-light photocatalysis in nitrogen-doped titanium oxides. *Science* 293: 269–271.
40. Mi L, Zhang Y, Wang PN (2008) First-principles study of the hydrogen doping influence on the geometric and electronic structures of N-doped TiO_2. *Chem Phys Lett* 458: 341–345.